NMR Structure of the Amino-Terminal Domain from the Tfb1 Subunit of TFIIH and Characterization of Its Phosphoinositide and VP16 Binding Sites[†,‡]

Paola Di Lello,[§,||] Bao D. Nguyen,[||,⊥] Tamara N. Jones,[@] Krzysztof Potempa,[@] Michael S. Kobor,[+] Pascale Legault,[§,@] and James G. Omichinski*[,§,@,#]

Département de Biochimie, Université de Montréal, Montréal, Quebec, Canada, Biomolecular NMR Facility, University of California, Irvine, California 92697, Departments of Biochemistry and Molecular Biology and of Chemistry, University of Georgia, Athens, Georgia 30602, and Department of Molecular and Cell Biology, University of California, Berkeley, California 94720

Received January 17, 2005; Revised Manuscript Received March 24, 2005

ABSTRACT: General transcription factor IIH (TFIIH) is recruited to the preinitiation complex (PIC) through direct interactions between its p62 (Tfb1) subunit and the carboxyl-terminal domain of TFIIEα. TFIIH has also been shown to interact with a number of transcriptional activator proteins through interactions with the same p62 (Tfb1) subunit. We have determined the NMR solution structure of the amino-terminal domain from the Tfb1 subunit of yeast TFIIH ($Tfb1_{1-115}$). Like the corresponding domain from the human p62 protein, $Tfb1_{1-115}$ contains a PH domain fold despite a low level of sequence identity between the two functionally homologous proteins. In addition, we have performed in vitro binding studies that demonstrate that the PH domains of Tfb1 and p62 specifically bind to monophosphorylated inositides [PtdIns(5)P and PtdIns(3)P]. NMR chemical shift mapping demonstrated that the PtdIns(5)P binding site on Tfb1 (p62) is located in the basic pocket formed by β-strands β5−β7 of the PH domain fold. Interestingly, the structural composition of the PtdIns(5)P binding site is different from the composition of the binding sites for phosphoinositides on prototypic PH domains. We have also determined that the PH domains from Tfb1 and p62 are sufficient for binding to the activation domain of VP16. NMR chemical shift mapping demonstrated that the VP16 binding site within the PH domain of Tfb1 (p62) overlaps with the PtdIns(5)P binding site on Tfb1 (p62). These results provide new information about the recognition of phosphoinositides by PH domains, and point to a potential role for phosphoinositides in VP16 regulation.

The assembly of RNA polymerase II (RNAP II)[1] and the general transcription factors (GTFs) required for basal transcription onto a DNA promoter is termed the transcription preinitiation complex (PIC) (*1*). The GTFs include TFIID, TFIIB, TFIIF, TFIIE, TFIIH, and, in many cases, TFIIA (*1*). RNAP II differs from RNAP I and RNAP III in that its largest subunit possesses a distinct repeating heptapeptide unit with the consensus sequence Y-S-P-T-S-P-S that defines its carboxyl-terminal domain (CTD) (*2*, *3*). To be recruited to the PIC, the CTD of RNAP II must be in the unphosphorylated form. The CTD of RNAP II is then extensively phosphorylated during the initiation phase of the transcription process, before the start of the elongation (*4*, *5*). A number of nuclear kinases have been reported to phosphorylate the CTD of RNAP II, including the cdk7 (Kin28) subunit of TFIIH (*6*).

Originally discovered in humans, TFIIH has also been identified in yeast (factor b), and the subunits of yeast and human TFIIH are highly homologous (*7*, *8*). TFIIH is composed of 10 subunits, and it is the only GTF that displays enzymatic activity, including DNA-dependent ATPase (*9*), ATP-dependent DNA helicase (*10*), and CTD kinase activities (*6*). Yeast and human TFIIH are highly homologous in both structure and function, and the subunits can be grouped into two subcomplexes termed the core and CAK subcomplexes. The core subcomplex consists of XPB (Ssl2), p62 (Tfb1), p52 (Tfb2), p44 (Ssl1), p34 (Tfb4), and TTDA (Tfb5), whereas the CAK subcomplex contains cdk7 (Kin28), cyclin H (Ccl1), and MAT1 (Tfb3) in humans (yeast components in parentheses). The two complexes are linked by the XPD (Rad3) subunit (*7*, *8*).

[†] This work was supported by National Institutes of Health Grant RO1 GM60298-01 (J.G.O. and P.L.) and American Cancer Society Grant RPG LBC-100183 (J.G.O.).

[‡] The coordinates for Tfb_{1-115} have been deposited in the Protein Data Bank as entry 1Y5O.

* To whom correspondence should be addressed: Département de Biochimie, Université de Montréal, C.P. 6128 Succursale Centre-Ville, Montréal, PQ, Canada H3C 3J7. Phone: (514) 343-7341. Fax: (514) 343-2210. E-mail: jg.omichinski@umontreal.ca.

[§] Université de Montréal.

[||] These authors contributed equally to this work.

[⊥] University of California, Irvine.

[@] Department of Biochemistry and Molecular Biology, University of Georgia.

[+] University of California, Berkeley.

[#] Department of Chemistry, University of Georgia.

[1] Abbreviations: RNAP II, RNA polymerase II; GTF, general transcription factor; CTD, carboxyl-terminal domain; TAD, transcriptional activation domain; HSQC, heteronuclear single-quantum coherence spectroscopy; PtdIns, phosphatidylinositol; PtdIns(3)P, phosphatidylinositol 3-phosphate; PtdIns(4)P, phosphatidylinositol 4-phosphate; PtdIns(5)P, phosphatidylinositol 5-phosphate; $PtdIns(3,4)P_2$, phosphatidylinositol 3,4-biphosphate; $PtdIns(3,5)P_2$, phosphatidylinositol 3,5-biphosphate; $PtdIns(4,5)P_2$, phosphatidylinositol 4,5-biphosphate; $PtdIns(3,4,5)P_3$, phosphatidylinositol 3,4,5-triphosphate; PIP, phosphatidylinositol phosphate.

10.1021/bi050099s CCC: $30.25
Published on Web 04/30/2005

TFIIH is recruited to the PIC through interactions between its p62 (Tfb1) subunit and the acid-rich carboxyl-terminal domain of TFIIEα. This interaction leads to a marked increase in the extent of phosphorylation of the CTD of RNAP II by the cdk7 subunit of TFIIH (*11*). TFIIH has also been shown to interact with a number of activators through direct interactions with its p62 (Tfb1) subunit. Both p62 and Tfb1 have been shown to interact with the transcriptional activation domains (TADs) from VP16, p53, E2F-1, and the HIV-1 Tat protein (*12*−*14*). Interestingly, the interaction of these TADs with p62 (Tfb1) correlates with their ability to stimulate initiation and elongation (*13*).

The structure of the amino-terminal domain of p62 ($p62_{1-108}$) has recently been determined by nuclear magnetic resonance (NMR) spectroscopy and shown to contain a pleckstrin homology (PH) domain fold (*15*). In this paper, we describe the NMR structure of the amino-terminal domain from the Tfb1 ($Tfb1_{1-115}$) subunit of yeast TFIIH. $Tfb1_{1-115}$ contains a PH domain that is very similar to the PH domain of $p62_{1-108}$, which is consistent with the fact that these two proteins carry out homologous functions in yeast and humans. In addition, we have performed in vitro binding studies demonstrating that the PH domains of Tfb1 and p62 specifically bind to monophosphorylated inositides [PtdIns(5)P and PtdIns(3)P]. We used NMR chemical shift mapping to identify the binding pocket of PtdIns(5)P and VP16 on $Tfb1_{1-115}$. Interestingly, we found considerable overlap between the VP16 binding site and the binding site for PtdIns(5)P. Our results provide new structural information about the recognition of acidic TADs involved in transcriptional regulation, and suggest a potential role for phosphoinositides in VP16 regulation.

EXPERIMENTAL PROCEDURES

Cloning of Recombinant Proteins. The GST−$p62_{1-127}$ fragment was generated by starting with the GST−$p62_{1-548}$ DNA from the pGEX-2T (Amersham) vector (gift from J. Laadias, Harvard University, Cambridge, MA) and creating a blunt end at amino acid 127. The GST−$Tfb1_{1-115}$ fragment was inserted into a pGEX-2T plasmid vector. The GST−$VP16_{412-456}$ fragment was generously donated by S. Triezenberg (Michigan State University, East Lansing, MI).

Expression and Purification of Glutathione S-Transferase (GST) Fusion Proteins. The GST−$Tfb1_{1-115}$ and GST−$p62_{1-127}$ proteins used in the in vitro binding experiments were expressed in *Escherichia coli* host strain TOPP2 (Stratagene). The cells were grown at 37 °C, and protein expression was induced for 3 h at 30 °C with 0.7 mM isopropyl D-thiogalactoside (IPTG). The cells were harvested by centrifugation and resuspended in EBC buffer [50 mM Tris-HCl (pH 8.0), 120 mM NaCl, 0.5% NP-40, and 2 mM DTT]. The cells were then lysed by being passed through a French press and centrifuged at 100,000*g* for 45 min. The supernatant from the centrifugation was incubated for 1 h with 3 mL of glutathione−Sepharose (GSH) resin (Amersham) at 4 °C. Following incubation, the resin was collected by centrifugation and washed twice with NETN buffer [20 mM Tris-HCl (pH 8.0), 100 mM NaCl, 1 mM EDTA, 0.5% NP-40, 0.05% SDS, and 1 mM DTT] and once in phosphate-buffered saline (PBS) (10 mM Na_2HPO_4, 2 mM KH_2PO_4 (pH 7.4), 140 mM NaCl, and 3 mM KCl). The fusion protein was eluted off the resin by rotating for 10 min in elution buffer [50 mM Tris-HCl (pH 8.0), 100 mM NaCl, 1 mM DTT, and 15 mM reduced glutathione]. The eluted fusion protein was dialyzed into freezing buffer [50 mM Tris-HCl (pH 8.0), 100 mM NaCl, 20% glycerol, and 2 mM DTT] and stored at −80 °C.

Protein Expression and Purification for NMR Studies. $Tfb1_{1-115}$ and $p62_{1-127}$ were expressed as GST fusion proteins in *E. coli* host strain TOPP2. Uniform (>98%) ^{15}N-labeling and $^{15}N/^{13}C$-labeling were obtained by growing the cells in a modified minimal medium containing $^{15}NH_4Cl$ and [$^{12}C_6$]-glucose or [$^{13}C_6$]-glucose as the sole nitrogen and carbon sources, respectively. The cells were grown at 37 °C and induced for 4 h with 0.7 mM IPTG at 30 °C. The proteins were cleaved from the GST tag with thrombin, and the purification procedure was essentially identical to the procedure used for purifying the carboxyl-terminal domain of RAP74 (*16*).

The GST−$VP16_{412-456}$ fragment was expressed as a GST fusion protein in *E. coli* host strain TOPP2. The cells were grown at 37 °C, and protein expression was induced for 4 h with 0.7 mM IPTG at 30 °C. The cells were harvested by centrifugation, resuspended in GST lysis buffer [20 mM Tris-HCl (pH 7.4), 1 mM EDTA, 1 M NaCl, and 1 mM DTT], lysed by being passed through a French press, and centrifuged at 100,000*g* for 45 min. The supernatant was incubated for 1 h with 10 mL of GSH resin at 4 °C. Following incubation, the resin was washed with lysis buffer three times followed by equilibration with PBS (pH 7.4) containing 1 mM DTT. The resin containing the bound fusion protein was then incubated overnight at 25 °C with 100 units of factor Xa (Calbiochem) to cut the $VP16_{412-456}$ fragment from the GST. Following enzyme cleavage, the supernatant was incubated for 1 h with benzamidine−Sepharose (Amersham), filtered to remove the benzamidine−Sepharose, dialyzed into buffer A [20 mM phosphate buffer (pH 6.5), 1 mM DTT, and 1 mM EDTA], and then applied to a Q-Sepharose High Performance (Amersham) column (75 mL) equilibrated with buffer A. The $VP16_{412-456}$ fragment was eluted from the column using a gradient (from 0 to 100% over 700 mL) of buffer B [20 mM phosphate buffer (pH 6.5), 1 mM DTT, 1 mM EDTA, and 1 M NaCl]. Fractions containing purified $VP16_{412-456}$ were then pooled, dialyzed overnight into buffer A, and concentrated for NMR studies.

Samples for NMR Spectroscopy. The NMR samples were as follows. (1) For studies of the structure of free $Tfb1_{1-115}$, the sample consisted of 1.2 mM $Tfb1_{1-115}$ (unlabeled, ^{15}N-labeled, and $^{15}N/^{13}C$-labeled) in 20 mM sodium phosphate (pH 6.5) and 1 mM EDTA (100% D_2O or 90% H_2O/10% D_2O). (2) For titration of $Tfb1_{1-115}$ with dihexanoyl-PtdIns(5)P (Echelon), the sample consisted of 0.3 mM $Tfb1_{1-115}$ (^{15}N-labeled) in 2.5 mM sodium phosphate (pH 6.5) and 1 mM EDTA (90% H_2O/10% D_2O). PtdIns(5)P was added in increments from 0 to 0.45 mM. (3) For the studies of $p62_{1-127}$ with Ins(1,5)P_2, the sample consisted of 0.3 mM $p62_{1-127}$ (^{15}N-labeled) in 0.5 mM sodium phosphate (pH 6.5), 100 mM NaCl, and 1 mM EDTA (90% H_2O/10% D_2O). Ins(1,5)P_2 was added in increments from 0 to 0.45 mM. (4) For titration of $Tfb1_{1-115}$ with $VP16_{412-456}$, the sample consisted of 0.3 mM $Tfb1_{1-115}$ (^{15}N-labeled) in 2.5 mM sodium phosphate (pH 6.5) and 1 mM EDTA (90% H_2O/10% D_2O). $VP16_{412-456}$ was added in increments from 0 to

0.6 mM. (5) For titration of $p62_{1-127}$ with $VP16_{412-456}$, the sample consisted of 0.3 mM $p62_{1-127}$ (^{15}N-labeled) in 2.5 mM sodium phosphate (pH 7.0), 100 mM NaCl, and 1 mM EDTA (90% H_2O/10% D_2O). $VP16_{412-456}$ was added in increments from 0 to 0.3 mM. (6) For titration of $Tfb1_{1-115}$ with dibutanoyl-PtdIns(3,5)P_2 (Echelon), the sample consisted of 0.3 mM $Tfb1_{1-115}$ (^{15}N-labeled) in 2.5 mM sodium phosphate (pH 6.5) and 1 mM EDTA (90% H_2O/10% D_2O). PtdIns(3,5)P_2 was added in increments from 0 to 0.6 mM. (7) For titration of $Tfb1_{1-115}$ with Ins(1,3,4,5)P_4 (Echelon), the sample consisted of 0.3 mM $Tfb1_{1-115}$ (^{15}N-labeled) in 2.5 mM sodium phosphate (pH 6.5) and 1 mM EDTA (90% H_2O/10% D_2O). Ins(1,3,4,5)P_4 was added in increments from 0 to 0.6 mM.

NMR Spectroscopy. NMR spectra were collected at 300 K on Varian Unity Inova 500, 600, and 800 MHz NMR spectrometers equipped with z pulsed-field gradient units and triple-resonance probes. The backbone and aliphatic side chain resonances (^{1}H, ^{15}N, and ^{13}C) were assigned using a combination of NMR experiments as previously described (*16*). Distance restraints were obtained from two- and three-dimensional NOESY experiments (*17*−*20*). The NMR data were processed with NMRPipe/NMRDraw (*21*) and analyzed with NMRView (*22*).

The dissociation constants (K_d) were estimated from the changes in both ^{1}H and ^{15}N chemical shifts as observed in the two-dimensional ^{1}H−^{15}N HSQC spectra of $Tfb1_{1-115}$ upon binding to PtdIns(5)P or $VP16_{412-456}$. The chemical shift changes, measured at various $Tfb1_{1-115}$/ligand ratios, were plotted versus the ligand concentration, and the results were fitted by nonlinear regression according to the following equation (*23*, *24*):

$$\Delta\delta = \Delta\delta_{max}\frac{K_d + [P] + [L] - \sqrt{(K_d + [P] + [L])^2 - 4[P][L]}}{2[P]}$$

where $\Delta\delta$ (*25*) is the chemical shift change at various $Tfb1_{1-115}$/ligand ratios, $\Delta\delta_{max}$ is the chemical shift change at saturation, K_d is the dissociation constant, and [L] and [P] are the ligand and protein concentrations, respectively.

Structure Calculation. Structures were calculated using the torsion angle molecular dynamics (TAD) protocol of CNS (*26*) starting from one extended structure with standard geometry. The protocol employed the conformational database potential derived from structure databases (*27*, *28*). From a total of 62 calculated structures, 50 of them satisfied all the experimental constraints with no NOE violation greater than 0.2 Å and no TALOS-derived dihedral angle (ϕ and ψ) violations greater than 2°. The quality of the structures was analyzed using PROCHECK-NMR (*29*) and MOLMOL (*30*). All figures representing structures were generated using MOLMOL (*30*) and GRASP (*31*).

Phosphatidylinositol Phosphate Binding Studies. Phosphatidylinositol phosphate (PIP) strips (Echelon) were blocked for 1 h at room temperature in Tris-buffered saline (TBS) containing 3% fatty acid free bovine serum albumin (BSA) (Sigma). The strips were then incubated for 2 h at 25 °C with purified GST, the GST−$Tfb1_{1-115}$ fusion protein, or the GST−$p62_{1-127}$ fusion protein at a final protein concentration of 0.5 μg/mL in TBS containing 3% fatty acid free BSA. Following the incubation, the unbound protein was removed, and the strips were washed three times with TBS containing 3% fatty acid free BSA to remove nonspecific protein binding. The bound protein was incubated with anti-GST−HRP conjugate RPN1236 antibody (Amersham), and bound antibodies were detected by chemiluminescence using the ECL-Plus kit (Amersham).

Table 1

restraints used for the structure calculations	
total no. of NOE distance restraints	1208
short-range (intraresidue)	249
medium-range ($\|i - j\| \leq 4$)	569
long-range ($\|i - j\| > 4$)	390
hydrogen bond	20
no. of dihedral angle restraints (ϕ, ψ)	124
structural statistics	
rms deviations from idealized geometry	
bonds (Å)	0.00210 ± 0.00004
angles (deg)	0.3271 ± 0.0033
impropers (deg)	0.1939 ± 0.0050
rms deviation from distance restraints (Å)	0.0188 ± 0.0005
rms deviation from dihedral restraints (deg)	0.1432 ± 0.0052
Ramachandran statistics (%)[a]	
residues in most favored regions	85.2
residues in additional allowed regions	12.8
residues in generously allowed regions	1.4
residues in disallowed regions	0.6
atomic pairwise rmsd (Å) for backbone atoms (C′, C^α, N)[b]	0.40 ± 0.07
atomic pairwise rmsd (Å) for all heavy atoms[b]	1.19 ± 0.08

[a] Based on PROCHECK-NMR analysis (*29*). [b] Only residues 4−64 and 85−112 were used for the rmsd calculation. Residues at the N-terminus (1−3), at the C-terminus (113−115), and in flexible loop (65−84) were not included in the calculation.

RESULTS AND DISCUSSION

$Tfb1_{1-115}$ Structure. The three-dimensional structure of $Tfb1_{1-115}$ was determined using a set of 1208 NOE-derived distance restraints [249 intraresidue, 569 medium-range ($|i - j| \leq 4$), and 390 long-range ($|i - j| > 4$)], 20 hydrogen-bond restraints, and 124 dihedral angle (ϕ and ψ) restraints (Table 1). The 20 hydrogen bond restraints were derived from the slowly exchanging amide protons. Dihedral angle restraints were obtained from analysis of $^1H^\alpha$, ^{15}N, $^{13}C^\alpha$, $^{13}C^\beta$, and ^{13}C′ chemical shifts using TALOS (*32*). The dihedral angle restraints derived from TALOS are set as $\phi \pm$ error (or $\psi \pm$ error), where the value of the errors used for structure calculations (from 20° to 50°) is twice that obtained from the TALOS analysis. Starting from an extended model of $Tfb1_{1-115}$, 62 structures were calculated and 50 were accepted because they had no distance restraint violation greater that 0.2 Å and no dihedral angle restraint violation greater than 2°. Among the 50 accepted structures, the 20 conformers with the lowest energies were selected for further analysis (Table 1).

$Tfb1_{1-115}$ presents the typical architecture of a pleckstrin homology (PH) domain (*33*, *34*), consisting of two β-sheets and one long amphipatic α-helix at the carboxyl terminus (Figure 1A). The backbone superimposition of the 20 lowest-energy NMR structures of $Tfb1_{1-115}$ is reported in Figure 1A. The pairwise rmsd for the ensemble, in the regions defined by residues 4−64 and 85−112, is 0.40 ± 0.07 Å for the backbone atoms and 1.19 ± 0.08 Å for all the heavy atoms. The first β-sheet (sheet A) is formed by strands β1 (residues 4−9), β2 (residues 12−19), β3 (residues 26−31), and β4 (residues 36−41). Strands β1 and β2 are connected

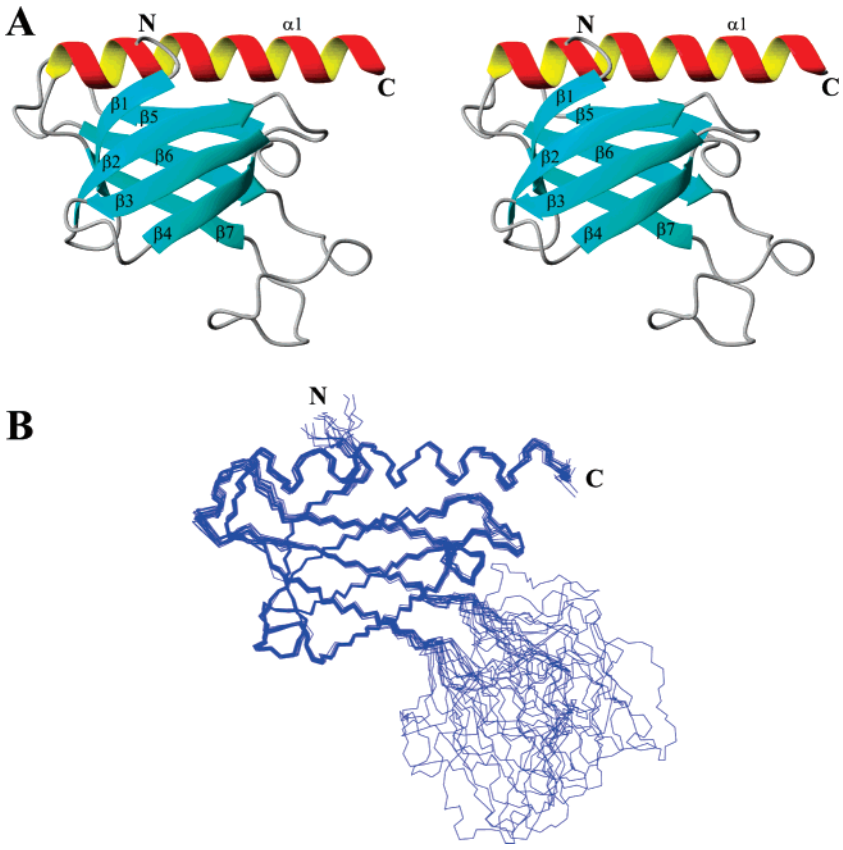

FIGURE 1: (A) Ribbon model for the lowest-energy conformer of $Tfb1_{1-115}$ shown in stereoview. (B) Overlay of the 20 lowest-energy structures of $Tfb1_{1-115}$. The structures were superimposed using C′, C^{α}, and N backbone atoms of residues 4−64 and 85−112.

by a βI′ turn (residues 9−12), whereas two loops (residues 20−25 and 32−35) connect strands β2 and β3 and β3 and β4, respectively. The second β-sheet (sheet B) consists of three strands spanning residues 47−50 (β5), 59−64 (β6), and 85−91 (β7). Strands β5 and β6 are joined by an eight-residue loop (residues 51−58), whereas strands β6 and β7 are linked by a long unstructured loop (residues 65−84).

A comparison of the $Tfb1_{1-115}$ structure with other PH domain structures revealed some variations in the prototypic PH scaffold. The major difference in PH domains is usually found in the composition of the three variable loops (VL1−VL3) connecting strands β1 and β2 (VL1), β3 and β4 (VL2), and β6 and β7 (VL3) (*35*−*37*). In most PH domains, the loop connecting β1 and β2 (VL1) is six or more residues and it is rich in basic amino acids. In $Tfb1_{1-115}$, this loop is a four-residue turn that contains only one basic residue (Lys^{11}). The other difference between Tfb1 and other PH domains occurs in the loop connecting strands β6 and β7 (VL3). $Tfb1_{1-115}$ contains a very long (20 residues) and flexible loop that is highly basic. In fact, almost all of the amino acids in this region have $^{15}N-^{1}H$ heteronuclear NOE values in the range of 0.13−0.40 (data not shown), indicating a high degree of backbone motion on the picosecond to nanosecond time scale. Long flexible loops such as this between β6 and β7 are rare in PH domains. In the case of Grp1 (general receptor for phosphoinositides-1), the corresponding loop is 26 residues long, but it is arranged in a twisted β-hairpin that extends the β-barrel from seven to nine strands (*38*).

Comparison of the Solution Structures of Yeast Tfb1 and Human p62. The solution structure of the amino-terminal domain of the human p62 subunit of TFIIH ($p62_{1-108}$) has recently been reported (*15*). Despite the low level of sequence identity (17.4%) in the first 120 amino acids (*39*), $Tfb1_{1-115}$ and $p62_{1-108}$ share the PH domain fold. The overlay between the backbone atoms (C^{α}, C′, and N) for residues in the secondary structure elements of the two proteins is 2.16 Å (data not shown). A feature peculiar to $Tfb1_{1-115}$ is the long flexible loop (residues 65−84) between β6 and β7 (VL3) which is replaced, in p62, by a four-residue turn. Overall, the yeast and human PH domains are very similar, and the major difference is the length of the connecting loop between β6 and β7.

Interaction of Tfb1 with Monophosphorylated Phosphoinositides. Like other PH domains, $Tfb1_{1-115}$ contains a positively charged surface on one face (Figure 2). Generally, the positively charged face enables PH domains to interact with phosphoinositides and/or negatively charged membranes (*33*). PH domains bind phosphoinositides with various affinities and specificities through interactions with the three positively charged variable loops (VL1−VL3) (*36*, *37*, *40*−*42*). For PH domains that bind with low affinity and specificity, phosphoinositide binding seems to be driven almost exclusively by nonspecific electrostatic interactions, and binding affinities correlate more with the number of phosphate groups than with their spatial arrangements (*37*). PH domains that bind with high affinity and specificity can be divided into subgroups on the basis of their selectivity for either PtdIns(4,5)P_2 or PtdIns(3,4,5)P_3. Those that bind better to 3-phosphoinositides that are products of the PI 3-kinase [PtdIns(3,4,5)P_3 and PtdIns(3,4)P_2] have also been shown to contain a characteristic sequence motif involving

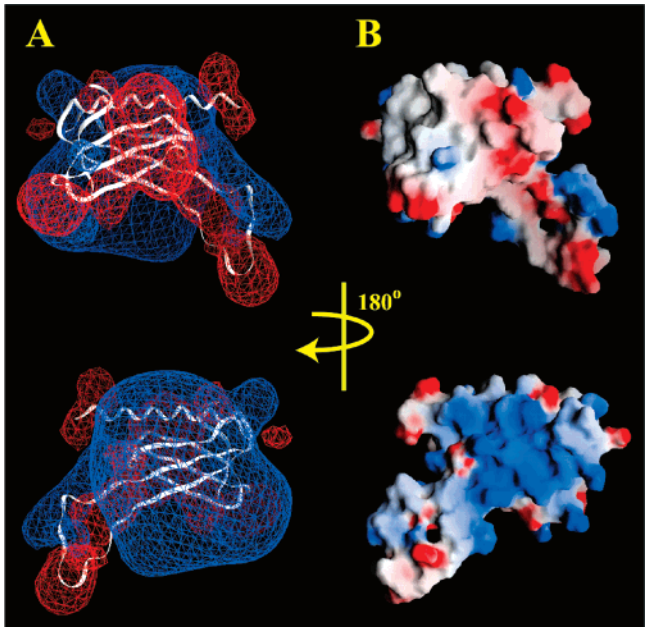

FIGURE 2: (A) Isopotential contours for the minimized average structure of $Tfb1_{1-115}$, plotted at −1.5 (red) and +1.5 kT (blue). The backbone C^{α} trace is shown as a ribbon. (B) Electrostatic potential for $Tfb1_{1-115}$, mapped on the molecular surface between −7 (red) and +7 kT (blue).

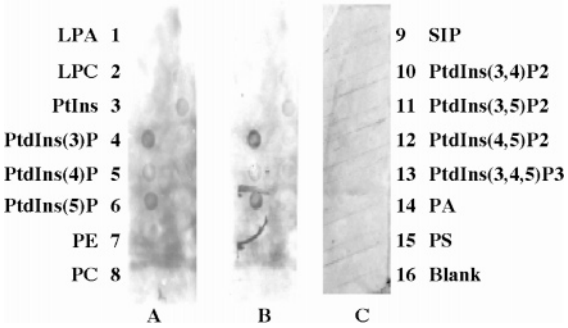

FIGURE 3: In vitro binding with PIP strips demonstrates that $Tfb1_{1-115}$ and $p62_{1-127}$ bind to monophosphorylated inositides. PIP strip blots (Echelon Biosciences) were incubated with (A) 1 μM GST−$Tfb1_{1-115}$ (B) 1 μM GST−$p62_{1-127}$, or (C) 1 μM GST. Each strip contains the 16 PIP analogues denoted at either side of the figure. Following washing to remove nonspecific binding, the bound proteins were detected with anti-GST−HRP conjugate (Amersham Biosciences): LA, lysophosphatidic acid; LPC, lysophosphocholine; PE, phosphatidylcholine; PI, phosphatidylinositol; SIP, sphingosine 1-phosphate; PA, phosphatidic acid; PS, phosphatidylcholine.

residues located in β1 and β2 and in the loop between them (VL1) (*43*). In $Tfb1_{1-115}$, the positively charged face is not centered around these three variable loops such as in prototypic PH domains, but rather, it is spread over strands β5−β7 of sheet B (Figure 2). Thus, it is clear that $Tfb1_{1-115}$ contains a positively charged face as seen in other PH domains, but within a distinctly different location.

Therefore, we examined the in vitro properties of Tfb1 ($Tfb1_{1-115}$) and p62 ($p62_{1-127}$) for binding to a series of phosphoinositides using a PIP strip assay. Tfb1 and p62 demonstrated preferential binding to monophosphorylated inositides, specifically, PtdIns(5)P and PtdIns(3)P (Figure 3), and unlike other PH domains, they failed to recognize either PtdIns(3,4)P_2 or PtdIns(3,4,5)P_3. In this regard, the binding properties of Tfb1 and p62 appear to be unique among the PH domains interacting with phosphoinositides. These results are not surprising given the structures of the PH domains of Tfb1 and p62. First, the PH domains of Tfb1 and p62 contain a positively charged face, but it is located in a different part of the fold from that of other PH domains. Second, the PH domains of Tfb1 and p62 lack the characteristic motif centered around VL1 that enables other PH domains to bind 3-phosphoinositide substrates with high affinity and specificity (*38*, *43*).

To map the phosphoinositide binding site of Tfb1 and to estimate the dissociation constant (K_d), we used NMR titration experiments to monitor the interaction between $Tfb1_{1-115}$ and PtdIns(5)P (*42*). Upon progressive additions of PtdIns(5)P to the free $Tfb1_{1-115}$, we observed continuous changes in ^{1}H and ^{15}N chemical shifts for several signals of $Tfb1_{1-115}$ in the two-dimensional ^{1}H−^{15}N HSQC spectra (Figure 4A). These chemical shift changes indicated the formation of a complex [$Tfb1_{1-115}$−PtdIns(5)P] in intermediate to fast exchange on the NMR time scale. The K_d for the $Tfb1_{1-115}$−PtdIns(5)P complex was estimated to be between 0.1 and 0.6 μM after analysis of the NMR titration curves of several Tfb1 residues (*23*, *24*). The residues from $Tfb1_{1-115}$ that showed the most significant changes in ^{1}H and ^{15}N chemical shifts upon formation of the complex {$\Delta\delta > 0.1$ ppm; $\Delta\delta = [(0.17\Delta N_H)^2 + (\Delta H_N)^2]^{1/2}$} (*25*) (Figure 4B) were mapped onto the NMR solution structure of $Tfb1_{1-115}$, revealing a novel mode of interaction of a PH domain with phosphoinositides (Figure 4C). The residues most affected by PtdIns(5)P binding are located in strand β5 (A^{50}), strand β6 (M^{59}, L^{60}, R^{61}, and L^{62}), strand β7 (H^{87}, M^{88}, F^{89}, S^{90}, and F^{91}), and the loop between β5 and β6 (T^{51}). The PtdIns(5)P binding site comprising β5−β7 and the loop between β5 and β6 is within the highly positively charged face of $Tfb1_{1-115}$ (Figures 2 and 4C), and this indicates that ionic interactions play an important role in the binding as expected. However, it is clear that other structural determinants must play a role in the interaction of $Tfb1_{1-115}$ with phosphoinositides, especially considering the high specificity with which $Tfb1_{1-115}$ recognizes PtdIns(5)P and PtdIns(3)P.

We also studied the interaction of $p62_{1-127}$ with phosphoinositides by NMR. Because of solubility problems of $p62_{1-127}$ in the presence of PtdIns(5)P, we examined the interaction of $p62_{1-127}$ with Ins(1,5)P_2, the soluble headgroup of PtdIns(5)P. Again, we observed changes in both ^{1}H and ^{15}N chemical shifts in the two-dimensional ^{1}H−^{15}N HSQC spectra of $p62_{1-127}$ upon addition of Ins(1,5)P_2 (Supporting Information Figure S1A) (*42*). We found that the residues displaying significant chemical shift changes cluster in a region that is centered on strands β5−β7 and in the loop between β5 and β6 (Figure 4D). On the basis of the structure of the PH domain of p62, it was predicted that a positively charged face involving lysine residues 60 and 62 in the loop between β5 and β6 as well as lysine residues 93 and 104 in the α-helix may be involved in ligand binding since these four lysines are highly conserved (*15*). The prediction of lysine 60 and 62 being involved is in agreement with our experimental results; however, the lysine residues in the α-helix (93 and 104) do not contribute to the binding of Ins(1,5)P_2. Therefore, the PH domains of Tfb1 and p62 not only have the same structural scaffold but also seem to share a recognition site for phosphoinositides. Interestingly, the PtdIns(5)P binding site on both Tfb1 and p62 appears to be unique among PH domains that bind phosphoinositides (see

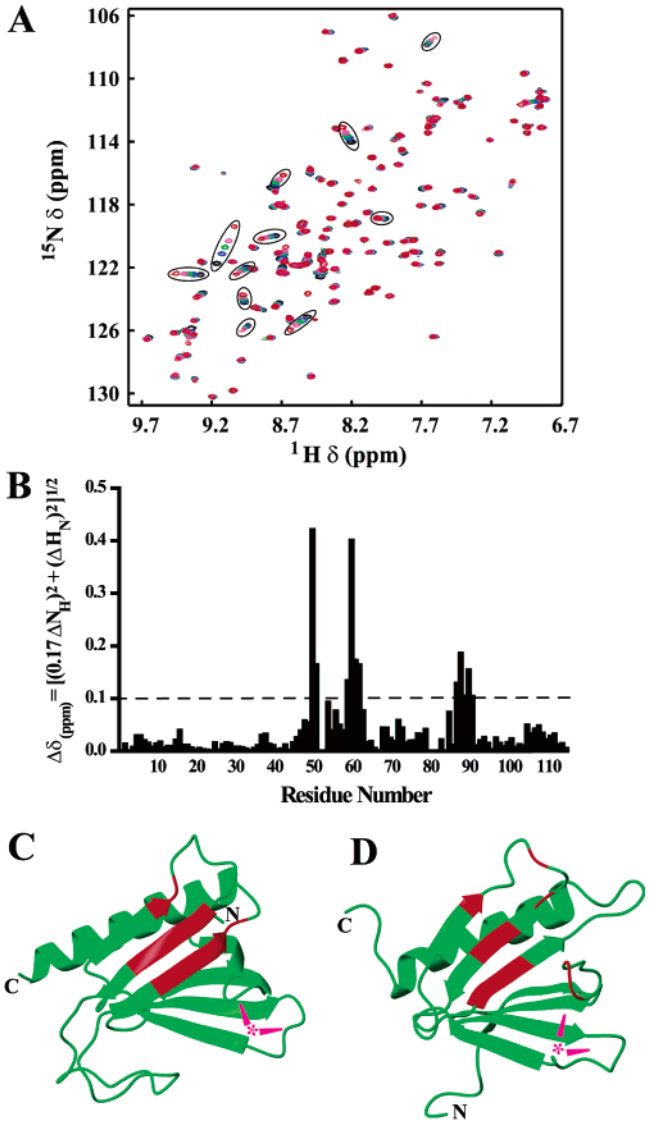

FIGURE 4: (A) Overlay of the two-dimensional ^{1}H−^{15}N HSQC spectra for ^{15}N-labeled Tfb1$_{1-115}$ in the free form (black) and in the presence of PtdIns(5)P [0.2 equiv (in blue), 0.4 equiv (in green), 0.6 equiv (in yellow), and 1.0 equiv (in red)]. The signals that undergo significant changes in ^{1}H and ^{15}N chemical shifts upon formation of the complex with PtdIns(5)P are highlighted in the black ovals. (B) Histogram of the variations in chemical shifts [$\Delta\delta_{(ppm)}$] (*25*) observed in the ^{1}H−^{15}N HSQC spectra of free Tfb1$_{1-115}$ and in the presence of 1 equiv of PtdIns(5)P. (C) The amino acids that undergo significant chemical shift changes [$\Delta\delta_{(ppm)} > 0.10$] upon formation of the Tfb1$_{1-115}$−PtdIns(5)P complex were mapped (in red) onto a ribbon model of the NMR structure of Tfb1$_{1-115}$. (D) Ribbon model of the free p62$_{1-108}$ structure (*15*). The residues showing large chemical shift changes in the two-dimensional ^{1}H−^{15}N HSQC spectra of p62$_{1-127}$ upon binding of Ins(1,5)P$_2$ are shown in red. In panels C and D, the location of the phosphoinositide binding site of DAPP1 is highlighted with pink asterisks (*47*). This is included to show the location of the prototypic phosphoinositide binding site in PH domains.

panels C and D of Figure 4 for comparison). To our knowledge, all of the other PH domains that interact with phosphoinositides have a characteristic binding site that comprises the variable loops connecting strands β1 and β2 (VL1), β3 and β4 (VL2), and β6 and β7 (VL3) which are located on a different face of the PH domain from strands β5−β7 and in the loop between β5 and β6 (*37*).

Interaction of Tfb1 with Polyphosphorylated Phosphoinositides. To examine the interaction of Tfb1 with polyphosphorylated phosphoinositides, NMR titration experiments with Tfb1$_{1-115}$ and PtdIns(3,5)P$_2$ and with Tfb1$_{1-115}$ and Ins(1,3,4,5)P$_4$ were performed (*42*). In the PIP strip assay, PtdIns(3,5)P$_2$ was the only polyphosphorylated phosphoinositide that demonstrated binding to Tfb1$_{1-115}$ and p62$_{1-127}$. Upon progressive additions of PtdIns(3,5)P$_2$ to ^{15}N-labeled Tfb1$_{1-115}$, we observed changes in ^{1}H and ^{15}N chemical shifts for several signals of Tfb1$_{1-115}$ in the two-dimensional ^{1}H−^{15}N HSQC spectra. These chemical shift changes indicated the formation of a complex [Tfb1$_{1-115}$−PtdIns(3,5)P$_2$] in intermediate to fast exchange on the NMR time scale. The K_d for the Tfb1$_{1-115}$−PtdIns(3,5)P$_2$ complex was estimated to be between 9 and 17 μM after analysis of the NMR titration curves of several Tfb1$_{1-115}$ residues (*23*, *24*). As was the case for PtdIns(5)P, the residues that showed the most significant changes in ^{1}H and ^{15}N chemical shifts upon formation of the Tfb1$_{1-115}$−PtdIns(3,5)P$_2$ complex {$\Delta\delta >$ 0.1 ppm; $\Delta\delta = [(0.17\Delta N_H)^2 + (\Delta H_N)^2]^{1/2}$} (*25*) are located in strands β5−β7 and in the loop between β5 and β6 (Supporting Information Figure S2A). This demonstrates that the binding site for PtdIns(3,5)P$_2$ is the same as the binding site for PtdIns(5)P. However, the affinity of Tfb1$_{1-115}$ appears lower for PtdIns(3,5)P$_2$ than for PtdIns(5)P (K_d values of 9−17 μM and 0.1−0.6 μM, respectively). Likewise, progressive additions of Ins(1,3,4,5)P$_4$ were made to the free Tfb1$_{1-115}$, and changes in ^{1}H and ^{15}N chemical shifts of Tfb1$_{1-115}$ were monitored in the two-dimensional ^{1}H−^{15}N HSQC spectra. In the titration with Ins(1,3,4,5)P$_4$, we failed to observe significant changes in ^{1}H and ^{15}N chemical shifts of Tfb1$_{1-115}$ that were indicative of formation of a specific complex {$\Delta\delta >$ 0.1 ppm; $\Delta\delta = [(0.17\Delta N_H)^2 + (\Delta H_N)^2]^{1/2}$} (*25*) (Supporting Information Figure S2B). These findings are consistent with the result from the PIP strip assay indicating that Tfb1$_{1-115}$ has a preference for monophosphorylated phosphoinositides, but that it also binds PtdIns(3,5)P$_2$. In addition, our NMR studies with the polyphosphorylated phosphoinositides verify that PtdIns(3,5)P$_2$ and PtdIns(5)P share a common binding site which is distinct from the prototypic PH domain phosphoinositide binding site involving the three variable loops, VL1−VL3 (*36*, *37*).

Interaction of Tfb1 and p62 with VP16. Both p62 and Tfb1 have been shown to interact with the TADs from VP16, p53, E2F-1, the estrogen receptor, and the HIV-1 Tat protein (*12*−*14*). Interestingly, a number of VP16 TAD mutants have been examined, and mutations within the amino-teminal subdomain of the VP16 TAD (VP16$_{412-456}$) appeared to affect significantly both transcriptional activation and binding of VP16 to Tfb1 (p62) (*13*, *44*). In addition, it has been demonstrated that the amino-terminal domain of p62 is required for interaction with the estrogen receptor (*45*). Therefore, we were interested in determining if the PH domains of Tfb1 and p62 were capable of binding specifically to VP16$_{412-456}$.

We used NMR chemical shift mapping to study the interaction of Tfb1$_{1-115}$ and p62$_{1-127}$ with VP16$_{412-456}$. Stepwise additions of VP16$_{412-456}$ to either Tfb1$_{1-115}$ or p62$_{1-127}$ resulted in continuous changes in ^{1}H and ^{15}N chemical shifts for several signals of Tfb1$_{1-115}$ and p62$_{1-127}$ in the two-dimensional ^{1}H−^{15}N HSQC spectra (Figure 5A and Supporting Information Figure S1B). This again indi-

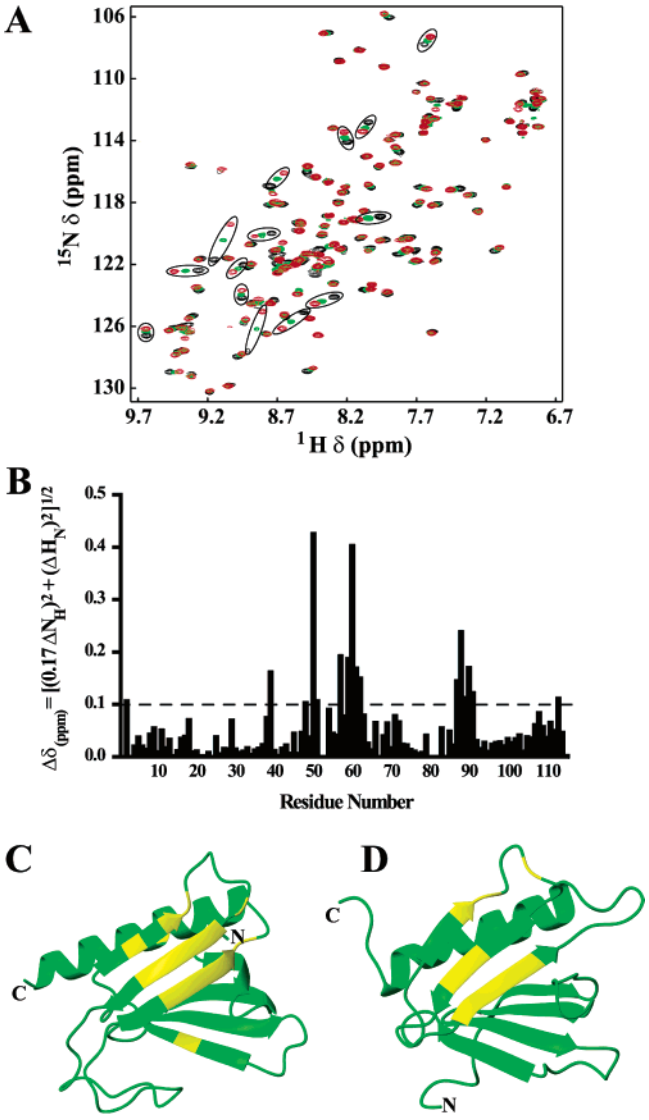

FIGURE 5: (A) Overlay of the two-dimensional ^{1}H−^{15}N HSQC spectra for ^{15}N-labeled Tfb1$_{1-115}$ in the free form (black) and in the presence of VP16$_{412-456}$ [0.5 equiv (in green) and 1.0 equiv (in red)]. (B) Histogram of the variation in chemical shift [$\Delta\delta_{(ppm)}$] (*25*) observed in the ^{1}H−^{15}N HSQC spectra of Tfb1$_{1-115}$ and in the presence of 1 equiv of VP16$_{412-456}$. (C) The amino acids that undergo a significant chemical shift change [$\Delta\delta_{(ppm)} > 0.10$] upon formation of the Tfb1$_{1-115}$−VP16$_{412-456}$ complex were mapped (in yellow) onto a ribbon model of the Tfb1$_{1-115}$ structure. (D) Ribbon model of the free p62$_{1-108}$ structure (*15*). The residues that undergo a significant chemical shift change in the two-dimensional ^{1}H−^{15}N HSQC spectra of p62$_{1-127}$ upon formation of the complex with Ins(1,5)P are shown in yellow.

cated the formation of complexes (Tfb1$_{1-115}$−VP16$_{412-456}$ and p62$_{1-127}$−VP16$_{412-456}$) in intermediate to fast exchange on the NMR time scale. The K_d for the Tfb1−VP16$_{412-456}$ complex was estimated to be between 4 and 7 μM after analysis of the NMR titration curves of several Tfb1$_{1-115}$ residues (*23*, *24*). The residues that exhibited the most significant changes in ^{1}H and ^{15}N chemical shifts upon formation of both complexes with VP16$_{412-456}$ {$\Delta\delta > 0.1$ ppm; $\Delta\delta = [(0.17\Delta N_H)^2 + (\Delta H_N)^2]^{1/2}$} (*25*) were located in the regions of strands β5−β7 and in the loop between β5 and β6 (Figure 5B). When mapped onto the NMR solution structure of Tfb1$_{1-115}$ (p62$_{1-108}$), the residues displaying significant chemical shift changes revealed that the VP16$_{412-456}$ binding site on Tfb1$_{1-115}$ (p62$_{1-108}$) (Figure 5C, D) is virtually identical to that of PtdIns(5)P (Figure 4C, D). To our knowledge, this is the first example demonstrating that the phosphoinositide-binding region of a PH domain could also participate in specific protein−protein interactions. These findings suggest that VP16$_{412-456}$ and PtdIns(5)P could compete for binding to the PH domain of Tfb1 (p62) (Figure 6).

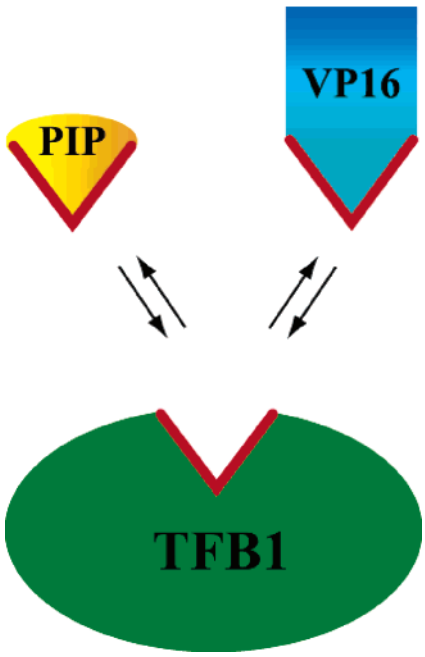

FIGURE 6: Cartoon highlighting the potential competitive binding between the activation domain of VP16$_{412-456}$ (VP16) and the monophosphorylated phosphoinositide PtdIns(5)P (PIP) for the PH domain of Tfb1 (TFB1).

CONCLUSION

In this work, we have determined the NMR solution structure of Tfb1$_{1-115}$, and we have used NMR methods to map the binding sites for both phosphoinositides and the TAD of VP16. The Tfb1 binding sites of both phosphoinositides and the TAD of VP16 are located on the positively charged face of the PH domain formed within strands β5−β7 and in the loop between β5 and β6 (Figures 4 and 5). Our biochemical and NMR studies have demonstrated that Tfb1$_{1-115}$ and p62$_{1-127}$ preferentially bind to monophosphorylated phosphoinositides [PtdIns(5)P and PtdIns(3)P]. The phosphoinositide binding site in Tfb1 (p62) also appears to be distinct from that of the prototypic PH domain. Furthermore, the phosphoinositide binding site in Tfb1 (p62) is distinct from that of other protein domains that bind phosphoinositides such as the ENTH domains, the FYVE domains, and the phox homology (PX) domains (*36*, *48*). Our results also suggest that the acidic activation domains of VP16$_{412-456}$ may compete with PtdIns(5)P for binding to the Tfb1 (p62) subunit of TFIIH.

Phosphoinositides are a diverse group of small molecule cellular regulators that originate from the membrane phospholipid, phosphatidylinositol (*48*−*50*), and have been implicated in regulating a number of important biological functions (*50*). It is clear that there is a nuclear phosphoinositide signaling network and that phosphoinositides play an important role in transcriptional regulation (*51*, *52*). In

addition, the concentration of various phosphoinositide analogues in the nucleus varies dramatically from one stage of the cell cycle to another (*53*). Recently, the chromatin-associated protein ING2 was shown to bind phosphoinositides through its PHD domain zinc finger (*51*). Interestingly, ING2 shows the same specificity for binding to phosphoinositides as Tfb1 and p62 (*51*). Extensive studies with ING2 demonstrated that PtdIns(5)P was the in vivo target of ING2 and that binding of PtdIns(5)P to ING2 regulates the activation of p53 by ING2 and p53-dependent apoptotic pathways (*51*).

We are currently carrying out additional NMR experiments to obtain three-dimensional structures of the $Tfb1_{1-115}$−PtdIns(5)P and $Tfb1_{1-115}$−$VP16_{412-456}$ complexes. The structures will allow us to further investigate the unusual mode of phosphoinositide recognition by the Tfb1 PH domain and how PtdIns(5)P and acidic TADs recognize the same binding site within this PH domain.

ACKNOWLEDGMENT

We acknowledge Hsin Chen for assistance in preparation of protein samples, Dr. Steven Triezenberg for the GST−$VP16_{412-456}$ clone, Dr. John Laadias for the GST−$p62_{1-548}$ clone, Dr. Frank Delaglio and Dr. Daniel Garrett for NMR data processing and analysis programs, and Dr. Lewis Kay for NMR pulse sequences and a modified version of CNS.

SUPPORTING INFORMATION AVAILABLE

Overlay of the two-dimensional $^1H-^{15}N$ HSQC spectra for ^{15}N-labeled $p62_{1-127}$ in the free form and in the presence of $Ins(1,5)P_2$ and overlay of the two-dimensional $^1H-^{15}N$ HSQC spectra for ^{15}N-labeled $p62_{1-127}$ in the free form and in the presence of $VP16_{412-456}$ (Figure S1). Histograms of the variations in chemical shifts [$\Delta\delta_{(ppm)}$] (*25*) observed in the $^1H-^{15}N$ HSQC spectra of free $Tfb1_{1-115}$ and in the presence of 2 equiv of $PtdIns(3,5)P_2$ and 2 equiv of $Ins(1,3,45)P_4$, respectively (Figure S2). This material is available free of charge via the Internet at http://pubs.acs.org.

REFERENCES

1. Hampsey, M. (1998) Molecular genetics of the RNA polymerase II general transcriptional machinery, *Microbiol. Mol. Biol. Rev. 62*, 465−503.
2. Allison, L. A., Moyle, M., Shales, M., and Ingles, C. J. (1985) Extensive homology among the large subunits of eukaryotic and prokaryotic RNA polymerases, *Cell 42*, 599−610.
3. Corden, J. L., Cadena, D. L., Ahearn, J. M., and Dahmus, M. E. (1985) A unique structure at the carboxyl terminus of the largest subunit of eukaryotic RNA polymerase II, *Proc. Natl. Acad. Sci. U.S.A. 82*, 7934−7938.
4. Lu, H., Flores, O., Weinmann, R., and Reinberg, D. (1991) The nonphophorylated form of the RNA polymerase II preferentially associates with the preinitiation complex, *Proc. Natl. Acad. Sci. U.S.A. 88*, 10004−10008.
5. O'Brien, T. S., Hardin, S., Greenleaf, A., and Lis, J. T. (1994) Phosphorylation of RNA polymerase II C-terminal domain and transcriptional elongation, *Nature 370*, 75−77.
6. Lu, H., Zawel, L., Fisher, L., Egly, J. M., and Reinberg, D. (1992) Human general transcription factor IIH phosphorylates the C-terminal domain of RNA polymerase II, *Nature 358*, 641−645.
7. Schultz, P., Fribourg, S., Poterszman, A., Mallouh, V., Moras, D., and Egly, J. M. (2000) Molecular structure of human TFIIH, *Cell 102*, 599−607.
8. Chang, W.-H., and Kornberg, R. D. (2000) Electron crystal structure of the transcription factor and DNA repair complex, core TFIIH, *Cell 102*, 609−613.
9. Conaway, R. C., and Conaway, J. W. (1989) An RNA polymerase II transcription factor has an associated DNA-depenent ATPase (dATPase) activity strongly stimulated by the TATA region of promoters, *Proc. Natl. Acad. Sci. U.S.A. 86*, 7356−7360.
10. Schaefer, L., Moncollin, V., Roy, R., Staub, A., Mezzina, M., Sarasin, A., Weeda, G., Hoeijmakers, J. H., Chambon, P., and Egly, J. M. (1993) DNA repair helicase: A component of BTF2 (TFIIH) basic transcription factor, *Science 260*, 58−63.
11. Ohkuma, Y., Hashimoto, S., Wang, C. K., Horikoshi, M., and Roeder, R. G. (1995) Analysis of the role of TFIIE in basal transcription and TFIIH-mediated carboxy-terminal domain phosphorylation through structure−function studies of TFIIEα, *Mol. Cell. Biol. 15*, 4856−4866.
12. Hengartner, C. J., Thompson, C. M., Zhang, J., Chao, D. M., Liao, S. M., Koleske, A. J., Okamura, S., and Young, R. A. (1995) Association of an activator with an RNA polymerase II holoenzyme, *Genes Dev. 15*, 897−910.
13. Blau, J., Xiao, H., McCracken, S., O'Hare, P., Greenblatt, J., and Bentley, D. (1996) Three functional classes of transcriptional activation domains, *Mol. Cell. Biol. 16*, 2044−2055.
14. Pearson, A., and Greenblatt, J. (1997) Modular organization of the E2F1 activation domain an its interaction with general transcription factors TBP and TFIIH, *Oncogene 15*, 2643−2658.
15. Gervais, V., Lamour, V., Jawhari, A., Frindel, F., Wasielewski, E., Dubaele, S., Egly, J.-M., Thierry, J.-C., Kieffer, B., and Poterszman, A. (2004) TFIIH contains a PH domain involved in DNA nucleotide excision repair, *Nat. Struct. Mol. Biol. 11*, 616−622.
16. Nguyen, B. D., Chen, H.-T., Kobor, M. S., Greenblatt, J., Legault, P., and Omichinski, J. G. (2003) Solution structure of the carboxyl-terminal domain of RAP74 and NMR characterization of the FCP1-binding sites of RAP74 and human TFIIB, *Biochemistry 42*, 1460−1469.
17. Bax, A., Sparks, S. W., and Torchia, D. A. (1989) Detection of insensitive nuclei, *Methods Enzymol. 176*, 134−150.
18. Marion, D., Kay, L. E., Sparks, S. W., Torchia, D. A., and Bax, A. (1989) Three-dimensional NMR of ^{15}N-labeled proteins, *J. Am. Chem. Soc. 111*, 1515−1517.
19. Pascal, S. M., Muhandiram, D. R., Yamazaki, T., Forman-Kay, J. D., and Kay, L. E. (1994) Simultaneous acquisition of ^{15}N- and ^{13}C-edited NOE spectra of proteins dissolved in H_2O, *J. Magn. Reson. 103*, 197−201.
20. Zuiderweg, E. R. P., McIntosh, L. P., Dahlquist, F. W., and Fesik, S. W. (1990) Three-dimensional carbon-13-resolved proton NOE spectroscopy of uniformly carbon-13-labeled proteins for the NMR assignment and structure determination of larger molecules, *J. Magn. Reson. 86*, 210−216.
21. Delaglio, F., Grzesiek, S., Vuister, G. W., Zhu, G., Pfeifer, J., and Bax, A. (1995) NMRPipe: A multidimensional spectral processing system based on UNIX pipes, *J. Biomol. NMR 6*, 277−293.
22. Johnson, B. A., and Blevins, R. A. (1994) NMRView: A computer program for the visualization and analysis of NMR data, *J. Biomol. NMR 4*, 603−614.
23. Morton, C. J., Pugh, D. J. R., Brown, E. L. J., Kahmann, J. D., Renzoni, D. A. C., and Campbell, I. D. (1996) Solution structure and peptide binding of the SH3 domain from human Fyn, *Structure 4*, 705−714.
24. Fielding, L. (2003) NMR Methods for the Determination of Protein−Ligand Dissociation Constants, *Curr. Top. Med. Chem. 3*, 39−53.
25. Farmer, B. T., Constantine, K. L., Goldfarb, V., Friedrichs, M. S., Wittekind, M., Yanchunas, J., Robertson, J. G., and Mueller, L. (1996) Localizing the $NADP^+$ binding site on the MurB enzyme by NMR, *Nat. Struct. Biol. 3*, 995−997.
26. Brunger, A. T., Adams, P. D., Clore, G. M., Gros, P., Grosse-Kunstleve, R. W., Jiang, J.-S., Kuszewski, J., Nilges, M., Pannu, N. S., Read, R. J., Rice, L. M., Simonson, T., and Warren, G. L. (1998) Crystallography and NMR system (CNS): A new software system for macromolecular structure determination, *Acta Crystallogr. D54*, 905−921.
27. Kuszewski, J., Gronenborn, A. M., and Clore, G. M. (1996) Improving the quality of NMR and crystallographic protein structures by means of a conformational database potential derived from structure databases, *Protein Sci. 5*, 1067−1080.
28. Choy, W.-Y., Tollinger, M., Mueller, G. A., and Kay, L. E. (2001) Direct structure refinement of high molecular weight proteins against residual dipolar couplings and carbonyl chemical shift

changes upon alignment: An application to maltose binding protein, *J. Biomol. NMR 21*, 31−40.
29. Laskowski, R. A., Antoon, J., Rullmann, C., Macarthur, M. W., Kaptein, R., and Thornton, J. M. (1996) AQUA and PROCHECK-NMR: Programs for checking the quality of protein structures solved by NMR, *J. Biomol. NMR 8*, 477−486.
30. Koradi, R., Billeter, M., and Wüthrich, K. (1996) MOLMOL: A program for display and analysis of macromolecular structures, *J. Mol. Graphics 14*, 51−55.
31. Nicholls, A., Sharp, K. A., and Honig, B. (1991) Protein folding and association: Insights from the interfacial and thermodynamic properties of hydrocarbons, *Proteins: Struct., Funct., Genet. 11*, 281−296.
32. Cornilescu, G., Delaglio, F., and Bax, A. (1999) Protein backbone angle restraints from searching a database for chemical shift and sequence homology, *J. Biomol. NMR 13*, 289−302.
33. Blomberg, N., Baraldi, E., Nilges, M., and Saraste, M. (1999) The PH superfold: A structural scaffold for multiple functions, *Trends Biochem. Sci. 24*, 441−445.
34. Lemmon, M. A., Ferguson, K. M., and Abrams, C. S. (2002) Pleckstrin homology domains and the cytoskeleton, *FEBS Lett. 513*, 71−76.
35. Haslam, R. J., Koide, H. B., and Hammings, B. A. (1993) Pleckstrin homology domain, *Nature 363*, 309−310.
36. Lemmon, M. A. (2003) Phosphoinositide recognition domains, *Traffic 4*, 201−213.
37. Lemmon, M. A., and Ferguson, K. M. (2000) Signal-dependent membrane targeting by pleckstrin homology (PH) domains, *Biochem. J. 350*, 1−18.
38. Lietzke, S. E., Bose, S., Cronin, T., Klarlund, J., Chawla, A., Czech, M. P., and Lambright, D. G. (2000) Structural basis of 3-phosphoinositide recognition by pleckstrin homology domains, *Mol. Cell 6*, 385−394.
39. Henikoff, S., and Henikoff, J. G. (1992) Amino acid substitution matrices from protein blocks, *Proc. Natl. Acad. Sci. U.S.A. 89*, 10915−10919.
40. Kavran, J. M., Klein, D. E., Lee, A., Falasca, M., Isakoff, S. J., Skolnik, E. Y., and Lemmon, M. A. (1998) Specificity and promiscuity in phosphoinositide binding by pleckstrin homology domains, *J. Biol. Chem. 273*, 30497−30508.
41. Dowler, S., Currie, R. A., Campbell, D. G., Deak, M., Kular, G., Downes, C. P., and Alessi, D. R. (2000) Identification of pleckstrin-homolgy-domain-containing proteins with novel phosphoinositide-binding specificities, *Biochem. J. 351*, 19−31.
42. Auguin, D., Barthe, P., Auge-Therese, M.-T., Stern, M.-H., Noguchi, M., and Roumestand, C. (2004) Solution structure and backbone dynamics of the pleckstrin homology domain of the human protein kinase B(PKB/Akt). Interaction with inositol phosphates, *J. Biomol. NMR 28*, 137−155.
43. Isakoff, S. J., Cardozo, T., Andreev, J., Li, Z., Ferguson, K. M., Abagyan, R., Lemmon, M. A., Aronheim, A., and Skolnik, E. Y. (1998) Identification and analysis of PH domain-containing targets of phosphatidylinositol 3-kinase using a novel in vivo assay in yeast, *EMBO J. 17*, 5374−5387.
44. Xiao, H., Pearson, A., Coulombe, B., Truant, R., Zhang, S., Regier, J. L., Trienzenberg, S. J., Reinberg, D., Flores, O., Ingles, C. J., and Greenblatt, J. (1994) Binding of basal transcription factor TFIIH to the acidic activation domain of VP16 and p53, *Mol. Cell. Biol. 14*, 7013−7024.
45. Chen, D., Riedl, T., Washbrook, E., Pace, P. E., Coombes, R. C., Egly, J.-M., and Ali, S. (2000) Activation of estrogen receptor a by S118 phosphorylation involves a ligand-dependent interaction with TFIIH and participation of CDK7, *Mol. Cell 6*, 127−137.
46. Ferguson, K. M., Lemmon, M. A., Schlessinger, J., and Sigler, P. B. (1995) Structure of the high affinity complex of inositol trisphosphate with a phospholipase C pleckstrin homology domain, *Cell 83*, 1037−1046.
47. Ferguson, K. M., Kavran, J. M., Sankaran, V. G., Fournier, E., Isakoff, S. J., Skolnik, E. Y., and Lemmon, M. A. (2000) Structural basis for discrimination of 3-phosphoinositides by pleckstrin homology domains, *Mol. Cell 6*, 373−384.
48. Prestwich, G. D. (2004) Phosphoinositide Signaling: From Affinity Probes to Pharmaceutical Targets, *Chem. Biol. 11*, 619−637.
49. Irvine, R. F. (2003) Twenty years of Ins(1,4,5)P3, and 40 years before, *Nat. Rev. Mol. Cell Biol. 4*, 586−590.
50. Clarke, J. H. (2003) Lipid Signalling: Picking Out the PIPs, *Curr. Biol. 13*, R815−R817.
51. Gozani, O., Karuman, P., Jones, D. R., Ivanov, D., Cha, J., Lugovskoy, A. A., Baird, C. L., Zhu, H., Field, S. J., Lessnick, S. L., Villasenor, J., Mehrotra, B., Chen, J., Rao, V. R., Brugge, J. S., Ferguson, C. G., Payrastre, B., Myszka, D. G., Cantley, L. C., Wagner, G., Divecha, N., Prestwich, G. D., and Yuan, J. (2003) The PHD finger of the chromatin-associated protein ING2 functions as a nuclear phosphoinositide receptor, *Cell 114*, 99−111.
52. Irvine, R. F. (2003) Nuclear lipid signalling, *Nat. Rev. Mol. Cell Biol. 4*, 349−361.
53. Clarke, J. H., Letcher, A. J., D'Santos, C. S., Halstead, J. R., Irvine, R. F., and Divecha, N. (2001) Inositol lipids are regulated during cell cycle progression in the nuclei of murine erythroleukaemia cells, *Biochem. J. 357*, 905−910.

BI050099S